OPEN ACCESS
Fractals, Vol. 30, No. 5 (2022) 2240185 (14 pages)

DOI: 10.1142/S0218348X22401855

GENERATION AND ROBUSTNESS OF QUANTUM MEMORY-ASSISTED ENTROPIC UNCERTAINTY AND UNCERTAINTY-INDUCED NONLOCALITY OF TWO NITROGEN-VACANCY CENTERS COUPLED BY OPEN TWO NANOCAVITIES

ABDEL-HALEEM ABDEL-ATY*
Department of Physics, College of Sciences
University of Bisha, P. O. Box 344
Bisha 61922, Saudi Arabia

Physics Department, Faculty of Science
Al-Azhar University, Assiut 71524, Egypt
amabdelaty@ub.edu.sa

ABDEL-BASET A. MOHAMED
Department of Mathematics
College of Science and Humanities in Al-Aflaj
Prince Sattam bin Abdulaziz University, Saudi Arabia

Department of Mathematics, Faculty of Science
Assiut University, Assiut, Egypt
abdelbastm@aun.edu.eg

ATTA UR RAHMAN
Key Laboratory of Aerospace Information
Security and Trusted Computing
Wuhan University, Wuhan 430072, P. R. China

*Corresponding author.

HICHEM ELEUCH
Department of Applied Physics and Astronomy
University of Sharjah, Sharjah, UAE
Department of Applied Sciences and Mathematics
College of Arts and Sciences
Abu Dhabi University, Abu Dhabi 59911, UAE
Institute for Quantum Science and Engineering
Texas A&M University
College Station, TX 77843, USA

Received October 12, 2021
Accepted January 2, 2022
Published August 25, 2022

Abstract

In this paper, we investigate the dynamics of quantum memory-assisted entropic uncertainty, uncertainty-induced nonlocality and log-negativity entanglement of two nitrogen-vacancy centers (NVC). In particular, we are interested in analyzing two nitrogen-vacancy centered qubits coupled with two coherent nanocavities. We consider two different configurations of NVC qubits: when the qubits are prepared initially in separable and maximally entangled states. We demonstrate that coherent nanocavities can be successfully used to generate nonlocality and entanglement in the two NVC qubits while suppressing the associated entropic uncertainty. When the system is considered initially in separable two-NVC qubits, we show that the coupled coherent nanocavities successfully generate nonlocality and entanglement while avoiding the associated entropic uncertainty. The parameter's adjustment determines the degree of entanglement, nonlocality generation, and preservation. In comparison, we find entanglement more vulnerable to the decoherence and entropic uncertainty action between the two NVC qubits and nanocavities than the uncertainty-induced nonlocality. Furthermore, the NVC-qubits coupled with two coherent nanocavities promote entanglement's sudden birth and death phenomena. This study contributes to the quantum mechanical protocols requiring the robust practical generation of entanglement and nonlocality as well as the related information preservation for the increased efficiency of quantum devices.

Keywords: Quantum Memory-Assisted Entropic Uncertainty; Uncertainty-Induced Non;ocality; Nitrogen-Vacancy Centers; Nanocavities.

1. INTRODUCTION

Variable theories cannot replicate all of quantum mechanics' conclusions. This emphasized the uniqueness of quantum state correlations, giving rise to the idea of quantum nonlocality.[1] Experiments on Bell inequalities,[2–7] have recently generated exciting results, as well as developments in quantum technology,[8,9] have sparked interest in this effect, which remains one of quantum mechanics' most difficult issues to tackle. Quantum nonlocality discloses the strong ties that bind numerous quantum particles, including some that transform their states rapidly when the state of others is observed, no matter how far apart they are. Aside from quantum nonlocality, the essential quantum information resources for quantum computation[10–14] include quantum coherence and nonclassical correlations, which are the key differences between quantum and classical physical systems.[15] Quantum device realization has been advanced significantly in recent years, with several applications in business and research.[16,17] It has been shown that the quantum computer can solve a variety of algorithms and sophisticated protocols that are impossible to accomplish with conventional computers.[18–21] Nearly all quantum computers require nonlocal features, such as quantum correlations.[22] As a result, quantum correlations, as well as the understanding of their resources and relative preservation, can benefit the advancement of quantum information processing and computing protocols.

Several challenges must be addressed to construct an effective quantum computer for quantum control, optimization, and other applications.[23,24] Preserving the quantum-correlated data created by the quantum procedures is one of the most arduous problems that researchers encounter. Quantum memory has been proposed using quantum dots,[25] nanoresonators,[26] NVC in Diamond,[27] and nanomechanical oscillator.[28,29] Because of its great physical qualities, such as long sustained coherence and a huge optical band gap, the NVC is one of the finest quantum storage solutions.[30,31] Jelezko *et al.* were the first to prepare diamond defects.[32–34] This experiment resulted in the development of several diamond defect applications, including nanoscale sensors,[35] the implementation of a photostable single-photon laser source,[36] optical preparation,[37] optical quantum networks,[38] and readout of defects in quantum materials as an electronic spin,[39] making the NVC the most suitable for quantum information technology and quantum memory. The NVC defects have been used in quantum register implementations that rely on the NVC electron spin and are close to the Nitrogen and carbon nuclear spins at room temperature. These achievements are the first step toward commercializing quantum storage. Steiner *et al.* carried out additional experiments to show the NVC's utility as a quantum memory.[40–42] In diamonds, they could make high-quality nitrogen defect quantum register spins. The suitability of NVC centers for quantum storage has been demonstrated using density functional theory tools to investigate their quantum properties.[31]

The interactions between solid-state emitters and high-Q nanocavities have sparked a lot of interest in quantum optics and quantum information science as a result of experimental developments in nanoscale photonic crystal (PC) cavity fabrication[43,44] and solid-state device design.[45,46] The diamond NVC,[47] which comprises a dopant nitrogen atom and a nearby vacancy, is a promising cornerstone for solid-state quantum computing at room temperature[48] due to long electronic and nuclear spin lifetimes and the potential for optical coherence encryption, such as fast initialization, well qubit readout, and information storage. Our work can be used for conceiving efficient quantum memory[49] and integrated optical sources,[50] plasmon-assisted light transmission[51] to mention a few. Note that in the current case, we mainly focus on the theoretical approach for the dynamics of correlations in NVC-qubits. The reason behind this is that the theoretical study can greatly provide insight into many considerable aspects of the problem.[52–56] In addition, based on results we provide insight into practical quantum computing, for example, the current set-up, we have devised can be used as efficient quantum memory with enhanced preservation time,[49] pulsed quantum frequency combs,[57] integrated optical micro-comb source,[50] memory associated with high-speed and scalable optical neural networks,[58] and in plasmon-assisted light transmission,[51] etc. We investigate a system of two open PC crystal cavities, each containing a coherently pumped NVC center. Each NVC center can only have a three-level configuration of the Λ type with a specific excited state.

In today's quantum emerging environment, more efficient and conveniently available quantum resources are necessary to carry out nonlocal protocols efficiently. As a result, we have been motivated to develop a theoretical setup that can be easily implemented for practical quantum computing and data processing protocols. The generation of quantum correlations and overcoming the entropy mixedness in all of the quantum system is the first step to deal with. In this study, we investigate the formation of quantum correlations in a system of two initial separable NVC qubits. The second critical step in the effective deployment of quantum protocols is the preservation and control of the generated quantum correlations.

This paper is organized as follows. In Sec. 2, the open NVC-nanocavity physical model and its evolution equations are presented. In Sec. 3, the definitions of the quantum memory-assisted entropic uncertainty, uncertainty-induced nonlocality and log-negativity entanglement are presented. Section 4 illustrates the numerical results and discussion of the dynamics of entropic uncertainty relations, the uncertainty generated nonlocality and log-negativity entanglement for two

NVC coupled with open nanocavities. Finally, the concluding section is presented in Sec. 5.

2. PHYSICAL MODEL

In this paper, we investigate a system consisting of two open and spaced photonic crystal cavities, each has inside a coherently-driven NV center.[43,59] Every NV center is assumed to be a Λ-type three-level system with the excited state $|E\rangle_k = (|e_+\rangle_k + |e_-\rangle_k)/\sqrt{2}(k = A, B)$ as an ancillary state, where $|e_\pm\rangle_k$ represents orbital states that have an angular momentum projection of ± 1 along the NV axis. In the case of low pumping, the excited state $|E\rangle_k$ decays to the ground states, $|0\rangle_k$ and $|1\rangle_k$ emitting photons with frequencies corresponding to the atomic transitions between the excited state and the ground states. Furthermore, we take into account: (1) the two nanocavities are coupled only because of the overlapping of their photonic wave functions. (2) the two nanocavities loss is restricted to the condition that no photon as a result of either spontaneous NV center emission or from the photonic crystal cavity leaking.[43] The effective interaction Hamiltonian of the system in the dispersive regime, where the cavity mode is off-resonant with all transitions of the NV centers, can be written as

$$
\begin{aligned}
\hat{H} = \sum_{k=A,B} & \chi_k \hat{\psi}_k^\dagger \hat{\psi}_k |0_k\rangle\langle 0_k| + \xi_k |1_k\rangle\langle 1_k| \\
& + \lambda_k (\hat{\psi}_k^+ |0_k\rangle\langle 1_k| + \hat{\psi}_k |1_k\rangle\langle 0_k|) \\
& - J(\hat{\psi}_1^\dagger \hat{\psi}_2 + \hat{\psi}_1 \hat{\psi}_2^\dagger) \\
& - \frac{i}{2}\sum_{j=1}^{2}[\gamma_j \hat{\psi}_j^\dagger \hat{\psi}_j - \kappa_j |e_j\rangle\langle e_j|], \qquad (1)
\end{aligned}
$$

$\chi_k = \frac{g_k^2}{\Delta_k}$ and $\xi_k = \frac{\Omega_k^2}{\Delta_k}$ design the coupling constants and $\lambda_k = \sqrt{\chi_k \xi_k}$ represents the effective Rabi frequency. $\hat{\psi}_k^\dagger(\hat{\psi}_k)$ are the creation (annihilation) matrix of the cavities with transition frequency ω. The first and the second terms reflect photon-induced and laser-induced dynamic energy shifts. J designs the two-nanocavity coupling in PC. γ_j and κ_j are the nanocavity dissipation rates and the spontaneous transitions between the two NVC state.

The non-Hermitian Schrödinger equation governs the system's evolution

$$
\frac{d}{dt}|\psi(t)\rangle = -i\hat{H}\,|\psi(t)\rangle, \qquad (2)
$$

$|\psi(t)\rangle$ is the time-dependent wave function. For the case of the one-excitation subspace, $|\psi(t)\rangle$ is represented as

$$
\begin{aligned}
|\psi(t)\rangle = \sum_{n=1}^{4} & [\Lambda_{n1}|00\rangle + \Lambda_{n2}|10\rangle + \Lambda_{n3}|01\rangle] \\
& \otimes |S_n\rangle, \qquad (3)
\end{aligned}
$$

where $\{|S_1\rangle = |1_A 1_B\rangle, |S_2\rangle = |1_A 0_B\rangle, |S_3\rangle = |0_A 1_B\rangle, |S_4\rangle = |0_A 0_B\rangle\}$ are the two NVC-qubits space.

By putting $\chi = \frac{1}{2}\gamma_k = \frac{1}{2}\kappa_k (k = A, B)$, the time-dependent coefficients $\Lambda_{nm}(m = 1{-}3)$ can be determined from Eq. (2) as

$$
\begin{aligned}
\dot{\Lambda}_{11} &= -i(\xi_A + \xi_B)\Lambda_{11} - i\lambda_B \Lambda_{22} - i\lambda_A \Lambda_{33} \\
&\quad - 2\chi\Lambda_{11}, \\
\dot{\Lambda}_{12} &= -i(\xi_A + \xi_B)\Lambda_{12} + iJ\Lambda_{13} - 3\chi\Lambda_{12}, \\
\dot{\Lambda}_{13} &= -i(\xi_A + \xi_B)\Lambda_{13} + iJ\Lambda_{12} - 3\chi\Lambda_{13}, \\
\dot{\Lambda}_{21} &= -i\xi_A \Lambda_{21} - i\lambda_A \Lambda_{43} - \chi\Lambda_{21}, \\
\dot{\Lambda}_{22} &= -i(\xi_A + \chi_B)\Lambda_{22} - i\lambda_B \Lambda_{11} + iJ\Lambda_{23} - 2\chi\Lambda_{22}, \\
\dot{\Lambda}_{23} &= -i\xi_A \Lambda_{23} + iJ\Lambda_{22} - 2\chi\Lambda_{23}, \\
\dot{\Lambda}_{31} &= -i\xi_B \Lambda_{31} - i\lambda_B \Lambda_{42} - \chi\Lambda_{31}, \\
\dot{\Lambda}_{32} &= -i\xi_B \Lambda_{32} + iJ\Lambda_{33} - 2\chi\Lambda_{32}, \\
\dot{\Lambda}_{33} &= -i(\chi_A + \xi_B)\Lambda_{33} + -i\lambda_A \Lambda_{11} + iJ\Lambda_{32} \\
&\quad - 2\chi\Lambda_{33}, \\
\dot{\Lambda}_{41} &= 0, \dot{\Lambda}_{42} = -i\chi_B \Lambda_{42} - i\lambda_A \Lambda_{31} \\
&\quad + iJ\Lambda_{43} - \chi\Lambda_{42}, \\
\dot{\Lambda}_{43} &= -i\chi_A \Lambda_{43} - i\lambda_A \Lambda_{21} + iJ\Lambda_{42} - \chi\Lambda_{43}.
\end{aligned} \qquad (4)
$$

We solve numerically Eq. (4), which allows us to explore the dynamics of quantum memory-assisted entropic uncertainty and uncertainty-induced nonlocality and log-negativity entanglement two NV centers.

3. QUANTUM MEMORY AND NONLOCALITY QUANTIFIERS

The dynamics of the entropic uncertainty, uncertainty induced nonlocality, and log-negativity are utilized to explore the generation and robustness of quantum memory and nonlocality by using the reduced two NVC density matrix

$$R^{AB}(t) = \mathrm{Tr}_{\mathrm{Nanocavity}}\{\psi(t)\rangle\langle\psi(t)|\}, \quad (5)$$

- **Entropic uncertainty**:
Bob's uncertainty regarding the outcome of the measurement is constrained by

$$S(P\,|\,B) + S(Q\,|\,B) \geq S(A\,|\,B) + \log_2 \frac{1}{c}, \quad (6)$$

where $S(A\,|\,B) = S(\hat{R}_{AB}) - S(\hat{R}_B)$ is the density operator's conditional von Neumann entropy $\hat{R}_{AB}$, $S(\hat{R}) = -\mathrm{tr}(\hat{R}\log_2 \hat{R})$. $S(X\,|\,B) = S(\hat{R}^{XB}) - S(\hat{R}_B)$, $X \in \{P, Q\}$ is the post measurement state and is defined as $\hat{R}^{XB} = \sum_x (|\psi_x\rangle\langle\psi_x| \otimes \mathbf{I})\hat{R}^{AB}(|\psi_x\rangle\langle\psi_x| \otimes \mathbf{I})$. Here $\hat{R}_B = \mathrm{tr}_A(\hat{R}^{AB})$ and $|\psi_x\rangle$ designs the eigenvectors of X and $\mathbf{I}$ is the identical operator.

The left and right sides of Eq. (6) can be represented as follows:

$$L(t) = S(\hat{R}_{\sigma_x B}) + S(\hat{R}_{\sigma_z B}) - 2S(\hat{R}_B), \quad (7)$$

$$R(t) = S(\hat{R}_{AB}) - S(\hat{R}_B) + 1, \quad (8)$$

where $L(t)$ and $R(t)$ are, respectively, the entropic uncertainty and its lower bound.

- *NVC-qubits uncertainty-induced nonlocality*
The UIN can be computed using the following formula[60] based on the skew information quantifier[61]:

$$\mathrm{UIN}(\hat{R}^{AB}) = \max_K I(\hat{R}^{AB}(t), K). \quad (9)$$

The $\mathrm{UIN}(\hat{R}^{AB})$ is determined by the maximal skew information of the NVC-qubits state $\hat{R}^{AB}(t)$ and local observable K. As an update to the preceding Eq. (9), it can be expressed as[61]

$$U(t) = \begin{cases} 1 - \lambda_{\min}(W_{AB}), & \mathbf{r} = 0; \\ 1 - \dfrac{1}{\|\mathbf{r}\|^2}\mathbf{r}\, W_{AB}\, \mathbf{r}^T, & \mathbf{r} \neq 0, \end{cases} \quad (10)$$

where $\|\mathbf{r}\|$ represents the Bloch vector norm $\mathbf{r}$.

- *Log-negativity entanglement:* Negativity and log-negativity are effective entanglement quantifiers.[62] We examine the entanglement for the bipartite NVC-qubits system R^{AB} using the log-negativity function[62]:

$$N(t) = \log_2[1 + 2n(t)], \quad (11)$$

where $n(t)$ represents the negativity defined as the absolute sum of negative eigenvalues of the matrix $(\hat{R}^{AB})^{T_A}$ (it represents the density matrix's partial transpose). The elements of $(\hat{R}^{AB})^{T_A}$ can be determined by

$$\langle i, j|(R^{AB})^{T_A}|m, n\rangle = \langle m, j|\hat{R}^{AB}|i, n\rangle. \quad (12)$$

The states are separable for $N(t) = 0$ and the function $N(t)$ is used to quantify the entanglement of the final state.

The dynamics of the quantum memory and nonlocality functions $L(t)$, $R(t)$ and $U(t)$ as well as $N(t)$ are calculated numerically by developing a MATLAB Program to compute the reduced two NVC density matrix elements of Eq. (5) at a time, which is used to compute the quantum memory and nonlocality functions by using Eqs. (7), (8), (10) and (11).

4. DYNAMICS OF TWO-NVC QUANTUM COHERENCE AND ENTANGLEMENT

In the NV centers' AB-qubit space: $\{|\varpi_k\rangle\}(k = 1-4)$, the reduced density of the two-NVC qubits can be expressed as

$$\hat{R}^{AB}(t) = \mathrm{Trace}_{\mathrm{Cav}}\{\hat{R}(t)\} = \sum_{j,k=1}^{4} \mathbf{V}_j \cdot \mathbf{V}_k, \quad (13)$$

where $\mathbf{V}_k = (\Lambda_{k1}\Lambda_{k2}\Lambda_{k3})$. In the following, the generation of quantum memory, nonlocality and entanglement of two NVC-qubits are explored for the case of the initial separable state

$$|\psi(0)\rangle_S = \frac{1}{\sqrt{3}}[|00\rangle \otimes |0\rangle + |10\rangle + |01\rangle] \otimes |S_2\rangle.$$

While the robustness of the quantum memory-assisted entropic uncertainty and the nonlocality is analyzed for the case of the maximally entangled state

$$|\psi(0)\rangle_E = \frac{1}{\sqrt{6}}[|00\rangle + |10\rangle + |01\rangle] \otimes [|S_1\rangle + |S_4\rangle].$$

4.1. Generation of Quantum Memory and Two NVC-Qubits Nonlocality

The dynamics of the generation of quantum memory-assisted entropic uncertainty and uncertainty-induced nonlocality beyond log-negativity nonlocality of two NVC qubits is investigated. We consider that the open NVC-nanocavity system

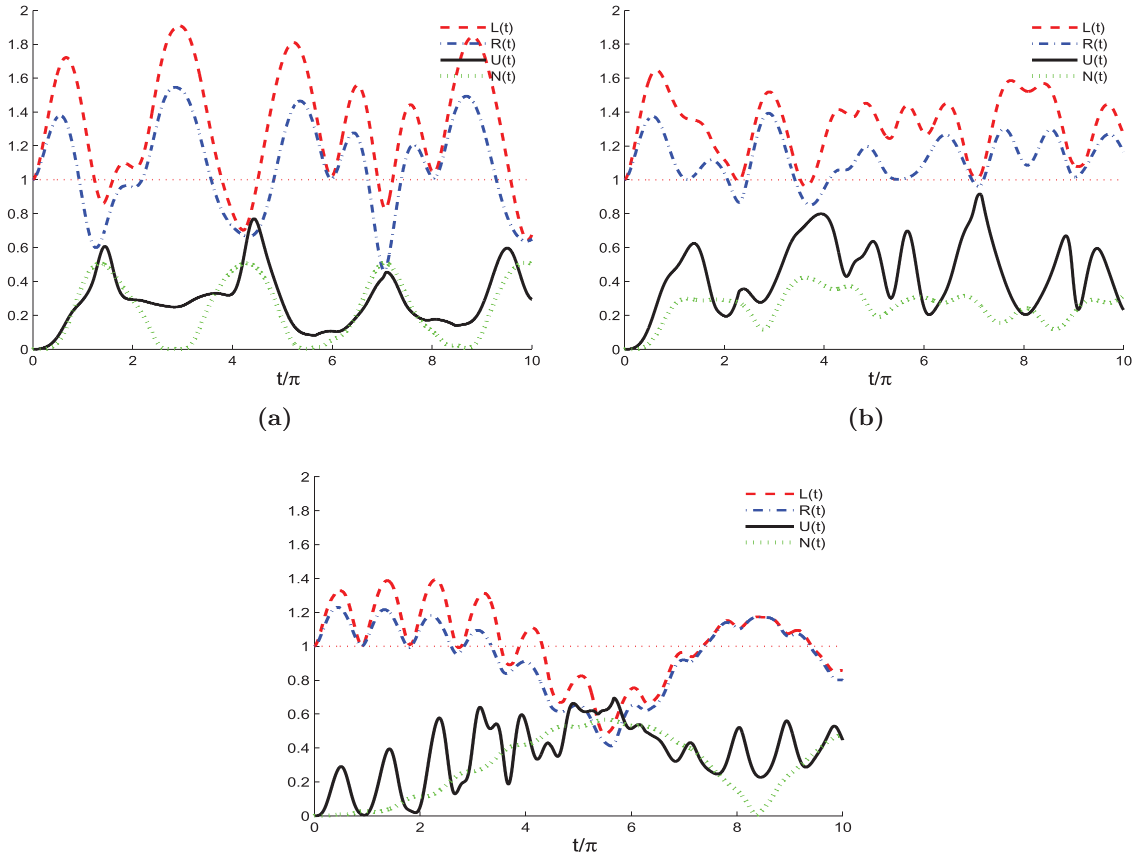

(a) (b) (c)

Fig. 1 The dynamics of the entropic uncertainty $L(t)$, entropic uncertainty lower bound $R(t)$, uncertainty-induced nonlocality $U(t)$, and log-negativity $N(t)$ for $|\psi(0)\rangle_S$ and $\chi_k = \xi_k = 0.5\lambda_k$ in the absence of the dissipation with different coupling cases: $J = 0.01\lambda_k$ in **(a)** $J = \lambda_k$ in **(b)** and $J = 4\lambda_k$ in **(c)**.

starts initially with the NVC-qubits separated state $|1_A 0_B\rangle$ as: $|\Psi(0)\rangle_S = \frac{1}{\sqrt{3}}[|00\rangle + |10\rangle + |01\rangle] \otimes ||1_A 0_B\rangle$.

The quantum memory-assisted entropic uncertainty and uncertainty-induced nonlocality, as well as log-negativity entanglement, are shown to be dependent on the NVC-nanocavity coupling in Fig. 1. Figure 1a, displays the dynamics of the quantum memory and nonlocality for the case $\chi_k = \xi_k = 0.5$ and $J = 0.01\lambda_k$ in the absence of the dissipation effect. In the current system–cavity coupling, the entropic uncertainty and entropic uncertainty lower bound are determined to be nonzero, and $L(t) = R(t) = 1$. This is exclusively due to the coupling of the uncorrelated state with the cavities. When the interaction between the NVC-qubits and nanocavities is activated, both functions achieve their peak. The $L(t)$, on the other hand, remains bigger and achieves its maximum quicker than the $R(t)$, proving that the $L(t) > R(t)$. Due to the back action of the nanocavities, the functions $L(t)$ and $R(t)$ are lowered to their minimum during later interaction time. Even though the NVC-qubits and nanocavities were separable initially, however, the entanglement and nonlocality grow to their maximum values for the latter interaction time. We also observe that the system's nonlocality is greater than its entanglement. None of the functions involved saturates to constant values and has a revival character at any point in time. As a consequence, it is essential to highlight that entanglement and nonlocality are successfully formed between the two NVC-qubits and nanocavities. At comparable periods, the minima of $L(t)$ and $R(t)$ correspond to the maxima of $U(t)$ and $N(t)$. This indicates that all the present phenomena under examination are in accord, and the results are consistent.

In Fig. 1b, the quantum memory and nonlocality functions $L(t)$, $R(t)$ and $U(t)$ as well as $N(t)$ are depicted for the parameter setting: $J = \lambda_k$ and $\chi_k = \xi_k = 0.5$. The coupling strength between the two connected nanocavities is raised in this example, and it is set to the unit strength of the effective Rabi-frequency λ_k. At $t = 0$, $L(t) = R(t) = 1$ and $N(t) = U(t) = 0$, as shown in Fig. 1b. However, as compared to Fig. 1a, the average entropic uncertainty appears to be smaller in this case. Furthermore, the $N(t)$ and $U(t)$ remain more resistant to the entropic and disorder effects of the NVC-nanocavities coupling and attain higher average values than that seen in Fig. 1a. All of this is due to the increasing coupling strength of the entangled nanocavities, which causes the NVC qubits to become entangled and encode nonlocality. In contrast to Fig. 1a, we observed a rise in revival character with time, indicating a successful flow of information, entanglement, and nonlocality between the NVC-qubits and two nanocavities.

For the case $J = 4\lambda_k$, the generation of the two NVC-qubit quantum memories and nonlocality is shown in Fig. 1c. Increased coupling strength between the two nanocavities has an impact on the generation of correlations between the NVC-qubits, as shown by the current parameter setup. For increasing interaction time choices, the dynamical map of entropic uncertainty relations appears to be completely different from that previously observed. The functions $L(t)$ and $R(t)$ increased uniformly between the time limits $0 \leq t/\pi \leq 3$ before decreasing to their minima. On the other hand, $N(t)$ and $U(t)$ started growing from zero to their highest points. There is a time interval where the minima of $L(t)$ and $R(t)$ meet the maxima of $N(t)$ and $U(t)$, $5.5 < t/\pi < 6.5$. During this time interval, the largest rise in entanglement and nonlocality, as well as the maximum drop in entropic action of the environments, occur. Every one of the quantifiers, except $N(t)$, shows a revival character.

The dependency of the generated two NVC-qubit quantum memory and nonlocality on the two NVC-qubit coupling constants χ_k and ξ_k is shown in Fig. 2. The current results address the enhanced interaction between NVC-qubits and nanocavities. These results differ from those depicted in Fig. 1. When the above-mentioned parameters are raised, the functions $L(t)$ and $R(t)$ exhibit a sudden rise from zero and grow with a rapid revival rate. $N(t) = U(t) = 0$, the entanglement and nonlocality functions, initially coincide, but later evolve to their different maxima and experience revivals. In comparison to the results in Fig. 1, the NVC-qubits interacting with the nanocavities are more correlated and exchange their features more quickly. As a result, χ_k and ξ_k have more prominent traces in coupled NVC-qubits and nanocavities for controlling entanglement and nonlocality than J and λ_k. In Fig. 2b, the entanglement and quantum memory generation duration were longer. Therefore, in the current system–environment coupling, longer entanglement and nonlocality values are favored by higher values of J and λ_k, as well as χ_k and ξ_k.

Figure 3 shows the effect of the dissipation on the dynamics of the quantum memory and the nonlocality when the dissipation rates $\chi_k = 0.025\lambda_k$. The recent results provide support to the hypothesis so that the coupling coefficient χ_k governs the growth map of quantum memory, entanglement, and entropic interaction dynamics. The assertion can be validated by looking at Figs. 2 and 3 for different values of χ_k. In both Figs. 3a and 3b, the entropic uncertainty relations graphs start from a

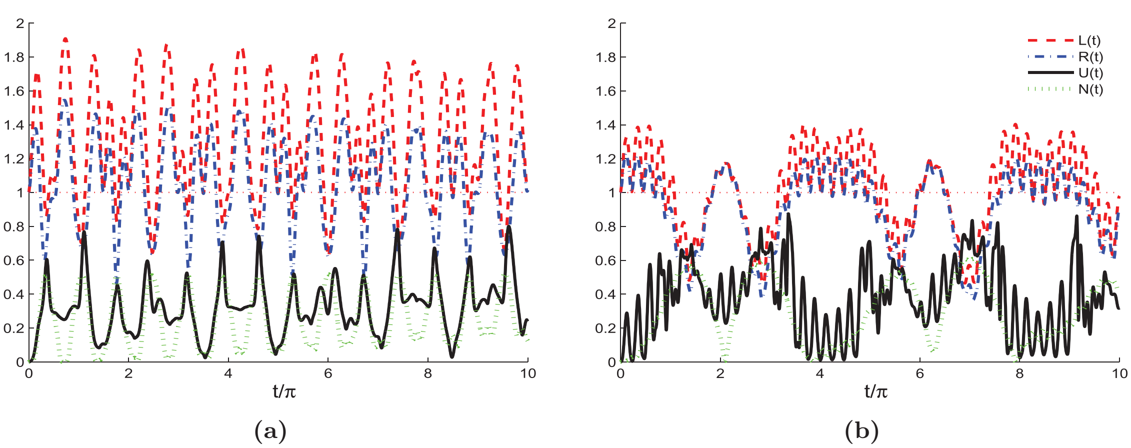

Fig. 2 The dynamics of the quantum memory and nonlocality functions $L(t)$, $R(t)$, $U(t)$, and $N(t)$ of Figs. 1a and 1c but for the case $\chi_k = \xi_k = 2\lambda_k$ in the absence of the dissipation effect.

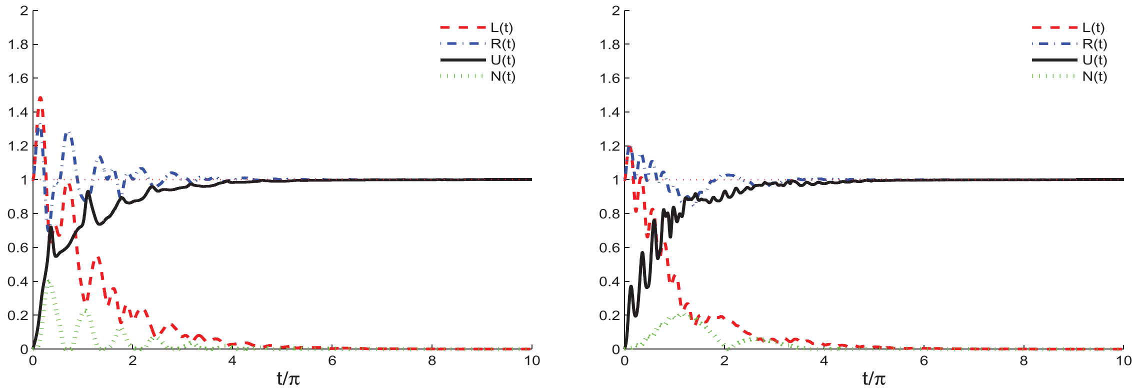

Fig. 3 The dynamics of the quantum memory and the nonlocality functions $L(t)$, $R(t)$, $U(t)$, and $N(t)$ of Fig. 2 but for the dissipation $\chi_k = 0.025\lambda_k$.

nonzero value, but they are soon suppressed by the formation of memory effects in the NVC-qubits, resulting in decreasing entropic actions. When the interaction is triggered, the quantifiers $N(t)$ and $U(t)$ that were previously zero (two uncorrelated NVC-qubits) achieve their maximum. Surprisingly, the behavior of the associated metrics diverges as the time of interaction rises. Unlike the $R(t)$ function, which uniformly declines to its original values, the $L(t)$ function hits 0 in its latter intervals. Entanglement and nonlocality function, $N(t)$ and $U(t)$, on the other hand, exhibited distinctive behavior. The first is uniformly decreasing to zero, whereas the second indicates that the quantum memory in the two NVC-qubits is effectively generated with high nonlocality. $U(t)$ reaches a final and stable saturation level as it rises over time. Despite the similarities between the two sides of Fig. 3, it is critical to highlight the differences in entanglement and quantum memory generation exchange rates. We note that the exchange rates between NVC-qubits and nanocavities improve as J increases. This could be observed in Fig. 3a.

4.2. Robustness of the Initial Quantum Memory, nonlocality and Entanglement

Here, the robustness of the initial quantum memory, nonlocality and entanglement in the two NVC-qubit systems will be analyzed when the NVC-nanocavity system state starts with the entangled state

$$|\psi(0)\rangle_E = \frac{1}{\sqrt{6}}[|00\rangle + |10\rangle + |01\rangle] \otimes [|S_1\rangle + |S_4\rangle].$$

For this case, the two nanocavities are initially in the correlated state $\frac{1}{\sqrt{3}}[|00\rangle + |10\rangle + |01\rangle]$ whereas the two NVC-qubits are initially in the entangled state $\frac{1}{\sqrt{2}}[|S_1\rangle + |S_4\rangle]$.

Figure 4 illustrates the robustness of the initial nonlocality and entanglement against the NVC-nanocavity interactions and entropic uncertainty with different cases of the NVC-nanocavity coupling. We set the values of $\chi_k = \xi_k$ and analyze the consequences of changing the value of the nanocavities intercoupling strength parameter J. We set $J = 0.01\lambda_k$ in Fig. 4a, and unlike the situations studied in Figs. 1–3, the system's entropic relations, $L(t) = R(t) = 0$. This is because the system is initially prepared in a maximally entangled state. The functions $N(t)$ and $U(t)$, on the other hand, start at their maximum values but $N(t) \neq U(t)$, with $N(t) = 0.8$ and $U(t) = 1$. The fact that $U(t) > N(t)$ and $L(t) > R(t)$ are in line with the preceding sections. The two nanocavities successfully preserved the initially encoded entanglement and nonlocality. Besides, at the final interaction time, the entanglement and nonlocality in the system, on the other hand, restore to their initial maximum levels. Except for entanglement, the correlations between the system and nanocavities rise and decrease within a specific time window and do not vanish completely. As a result, nanocavities appear to be a potential resource for reliable quantum memory and quantum correlations preservation and processing.

In Fig. 4b, we set the coupling strength of the nanocavities to $J = \lambda_k$. The modification of this value completely changes the dynamics of entropic

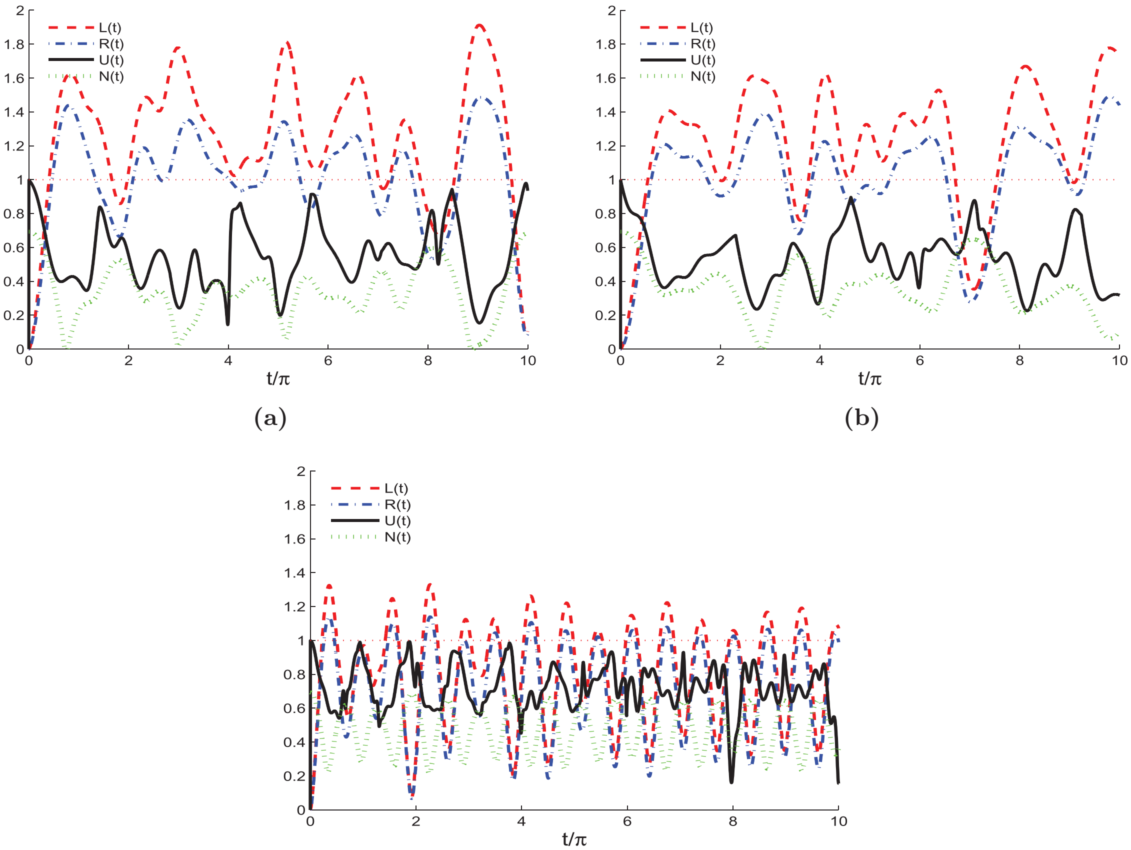

(a) (b) (c)

Fig. 4 The dynamics of the entropic uncertainty $L(t)$, entropic uncertainty lower bound $R(t)$, uncertainty-induced nonlocality $U(t)$, and log-negativity $N(t)$ for $|\psi(0)\rangle_E$ and $\chi_k = \xi_k = 0.5$ in the absence of the dissipation with different coupling cases: $J = 0.01\lambda_k$ in **(a)** $J = \lambda_k$ in **(b)** and $J = 4\lambda_k$ in **(c)**.

uncertainty relations, entanglement, and nonlocality. In terms of average entanglement and nonlocality preservation, the present parameter values for NVC-qubits and nanocavities are more effective. Unlike the $N(t)$ simulation in Fig. 1a, the $N(t)$ dynamics feature a single sudden death. Furthermore, in Fig. 1a, the $U(t)$ function remains above the highest value observed in Fig. 3a for the same measure. In both Figs. 1a and 1b, the $L(t)$ and $R(t)$ functions approach an extreme minimum, although in the current case, this occurs significantly faster. Entanglement and nonlocality become stronger as the coupling strength of the nanocavities increases.

The dynamics of uncertainty relations, entanglement, and uncertainty-induced nonlocality in two-NVC qubits coupled with two nanocavities are depicted in Fig. 4c. According to the dynamics of the functions $L(t)$ and $R(t)$, the entropic relations reach their maxima but suffer a larger loss than indicated in Figs. 4a and 4b. Furthermore, in previous cases, the maximum levels attained via entropic relations are far greater than in the current case. $N(t)$ and $U(t)$ experience a lesser loss, indicating greater entanglement and nonlocality preservation. It is important to highlight that the present revival rate in all functions is significantly greater. This indicates that the interchange of information and other types of quantum correlations between NVC-qubits and nanocavities improves as the intensity of the nanocavity coupling rises.

Figure 5 analyzes the dynamics of quantum memory-assisted entropic uncertainty and uncertainty-induced nonlocality beyond log-negativity for high NVC-qubit coupling constants. We notice a quick increase and decrease in the functions $L(t)$ and $R(t)$ beginning from zero for the current parameter set-up. Because the system's state is chosen to be maximally entangled, the entropic relations never vanish after the first increase. When the functions $N(t)$ and $U(t)$ are first decreased from their maximum values, a revival phenomenon occurs for the latter interaction time. The average level of

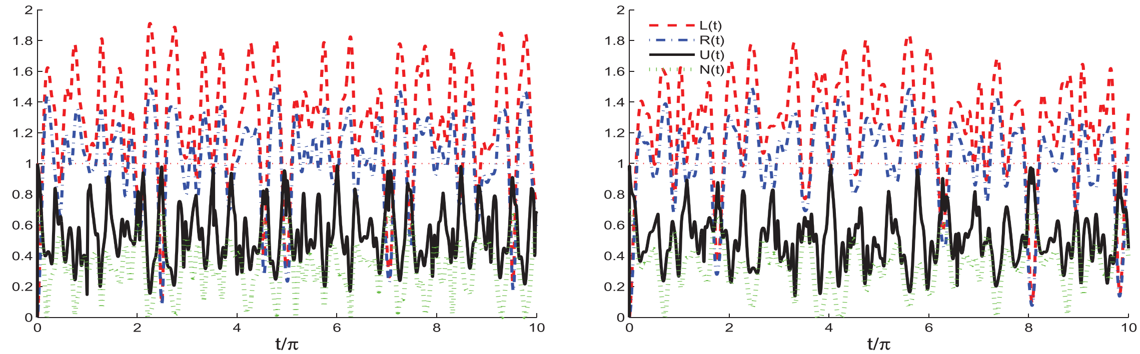

(a) (b)

Fig. 5 The dynamics of the quantum memory and the nonlocality functions $L(t)$, $R(t)$, $U(t)$, and $N(t)$ of Figs. 4a and 4b but for the case $\chi_k = \xi_k = 2$.

uncertainty appears to be higher in the current case than in Fig. 4, indicating that the coupling coefficients χ_k and ξ_k enhance the system's disorder rate. The system frequently becomes entirely disentangled with the least nonlocality due to the NVC-nanocavities interaction, but is then recovered. The dynamics of the currently involved functions remained the same in both Figs. 5a and 5b, however the latter case experiences the sudden death entanglement. This is due to an increase in the coupling strength between the two nanocavities, leading the system to become more entangled and nonlocal than in the previous case.

Figure 6 shows the effect of the dissipation on the quantum memory-assisted entropic uncertainty and uncertainty-induced nonlocality and log-negativity entanglement for the dissipation rates $\chi = 0.05\lambda_k$ and the large two-nanocavity coupling $J = 0.01\lambda_k$ with different dissipation NVC-qubits coupling constants: $\chi_k = \xi_k = 0.5$ in Fig. 6a and $\chi_k = \xi_k = 2$ in Fig. 6b. In the present figure, the entropic uncertainty relation functions, $L(t)$ and $R(t)$ develop quickly to their maxima and then decrease. Simultaneously, the entanglement and uncertainty-induced nonlocality functions, $N(t)$ and $U(t)$, fall to their first minimum and then increase again. When compared to Fig. 5, the revival phenomena are dramatically diminished during the whole interval. This implies that there is less contact between the two NVC-qubits and the two nanocavities. The average level of uncertainty-induced nonlocality appears to be higher than in Fig. 5, although entanglement remains suppressed under the present parameter settings. In accordance with $U(t)$, the $L(t)$ and $R(t)$ quantifiers attain lower values, reflecting less entropic uncertainty in the system. The results in Fig. 6b show that entanglement is significantly reduced when compared to

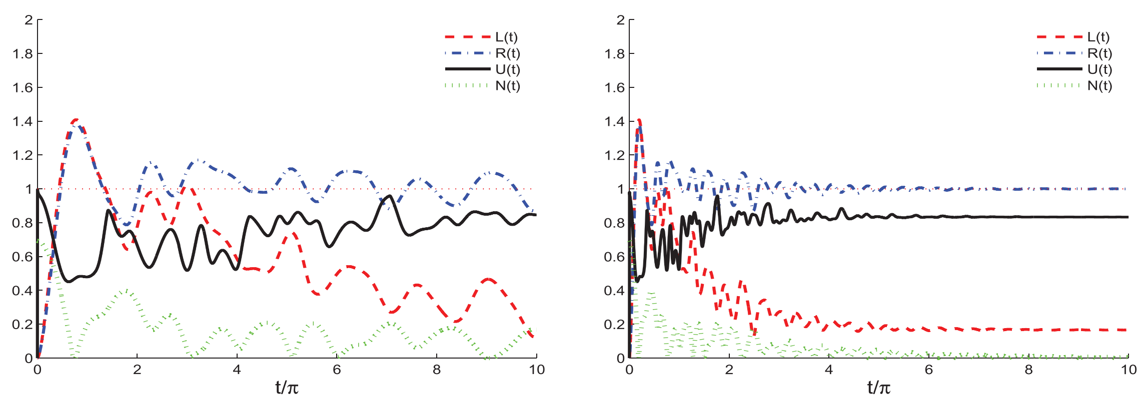

(a) (b)

Fig. 6 The dynamics of the quantum memory-assisted entropic uncertainty, uncertainty-induced nonlocality, and log-negativity nonlocality of Fig. 4a and 5a but for the dissipation $\chi = 0.05\lambda_k$.

nonlocality, which inevitably saturates at a greater constant level. The $L(t)$ function approaches a considerably lower saturation threshold in entropic uncertainty relations, whereas the $R(t)$ function recovers to its starting value. Despite this, the system's high resistance to uncertainty-based nonlocality cannot be ignored.

Finally, when two NVC qubits are connected with nanocavities, we have investigated the dynamics of entanglement, nonlocality, and entropic uncertainty relations. The dissipation effects are inevitable and induce loss of useful information in the current system. As a result, future contributions need to be on how to appropriately handle the nanocavities for the sake of practical applications.

In comparison to the induced nonlocality and entanglement defined for the NVC embedded in photonic crystal (PC) cavities,[63] we observe the induced nonlocality and entanglement suffer from high oscillations. Furthermore, the revival nature of quantum correlations in separated NVC embedded in PC cavities appears to be more periodic than the abrupt revival behavior seen for quantum dynamics in the current case.[43] The present physical model has the benefit of strongly supporting both generation and strong information exchange between NVC qubits and coupled coherent cavities; but, as shown in Ref. 64, quantum correlations can sometimes only display decay rather than generation. Quantum correlations can be attributed to the quantum channels with memory depicted in Ref. 65, but without the death and rebirth phenomena. Despite the differences in exact dynamical behavior, we discovered that the formation and stability of quantum correlations, as well as the suppression of entropic uncertainty, are similar to those described in Ref. 66.

5. CONCLUSIONS

We explored the dynamics of quantum memory-assisted entropic uncertainty, uncertainty-induced nonlocality, and log-negativity entanglement generation by two coupled dissipative nanocavities located between two Nitrogen-Vacancy centers (NVC). Each of the two nanocavities has been designed to provide a coherently-driven NVC. We have investigated the current physical system in two initial states: when it is prepared in a separable state and when it is maximally entangled. The generation of nonlocality and entanglement under the effect of two coupled nanocavities has been examined in the first case. In the second case, we have focused on the system's capacity to sustain entanglement and nonlocality while avoiding entropic uncertainty action. We have also performed a series of parameter changes and reported the results. The coupling of two NVC-qubits with two coherent nanocavities, according to our results, is one of the most promising quantum information science resources for successfully creating, transmitting, and preserving entanglement and nonlocality. We have demonstrated that the current system–environment coupling appears to be more resilient to entropic uncertainty and disordered behavior. The transformation of a separable state of two-NVC qubits and nanocavities into a highly nonlocal entangled state is possible. The design of the parameters influences various aspects of two-qubit NVC centres and nanocavities, such as entanglement, nonlocality, and related entropy suppression and generation. Their respective rates, and optimum outcomes can be achieved by parameter adjustment. As the coupling strength between the nanocavities grows, for example, the production of entanglement and nonlocality increases. In agreement, the related nonlocal correlations appear to be stronger and more robust to the entropic uncertainty relations when the coupling strength between the NVC-qubits and nanocavities is enhanced. Despite entanglement decreasing for the nonzero dissipation value, nonlocality remains robust against larger increases in entropic uncertainty relations. Even in the absence of entanglement, the system's uncertainty-induced nonlocality exists, showing that entanglement is more fragile than nonlocality. The ability to control the parameters that characterize the NVC-qubit nanocavities coupling may easily be exploited to provide optimized results. Thus, the current system-cavity design is a potential quantum information science resource for the effective transmission and long-term preservation of quantum information.

ACKNOWLEDGMENTS

The authors are very grateful to the referees for their constructive remarks, which have improved this paper. The authors extend their appreciation to the Deputyship for Research & Innovation, Ministry of Education in Saudi Arabia for funding this research work through the project number (IF-PSAU-2021/01/17712).

REFERENCES

1. T. Maudlin, *Quantum Non-Locality and Relativity*: *Metaphysical Intimations of Modern Physics* (John Wiley & Sons, 2011).
2. C. A. Melo-Luna, C. E. Susa, A. F. Ducuara, A. Barreiro and J. H. Reina, Quantum locality in game strategy, *Sci. Rep.* **7**(1) (2017) 1–11.
3. T. Van Himbeeck, J. B. Brask, S. Pironio, R. Ramanathan, A. B. Sainz and E. Wolfe, Quantum violations in the Instrumental scenario and their relations to the Bell scenario, *Quantum* **3** (2019) 186.
4. S. L. Braunstein and C. M. Caves, Wringing out better Bell inequalities, *Ann. Phys.* **202**(1) (1990) 22–56.
5. D. Aerts, S. Aerts, J. Broekaert and L. Gabora, The violation of Bell inequalities in the macroworld, *Found. Phys.* **30**(9) (2000) 1387–1414.
6. A. Tavakoli, N. Gisin and C. Branciard, Bilocal Bell inequalities violated by the quantum Elegant Joint Measurement, *Phys. Rev. Lett.* **126**(22) (2021) 220401.
7. J. D. Bancal, N. Gisin and S. Pironio, Looking for symmetric Bell inequalities, *J. Phys. A*, *Math. Theor.* **43**(38) (2010) 385303.
8. C. Erven, E. Meyer-Scott, K. Fisher, J. Lavoie, B. L. Higgins, Z. Yan and K. J. Resch, Experimental three-photon quantum nonlocality under strict locality conditions, *Nat. Photon.* **8**(4) (2014) 292–296.
9. R. A. Bertlmann and A. Zeilinger (eds.), *Quantum* (*un*) *Speakables*: *From Bell to Quantum Information* (Springer Science and Business Media, 2013).
10. M. A. Nielsen and I. L. Chuang, *Quantum Computation and Quantum Information* (Cambridge University Press, Cambridge, 2000).
11. A.-S. F. Obada, H. A. Hessian, A.-B. A. Mohamed and A. H. Homid, Efficient protocol of N-bit discrete quantum Fourier transform via transmon qubits coupled to a resonator, *Quantum Inf. Process.* **13** (2014) 475.
12. A.-B. A. Mohamed and H. Eleuch, Quantum correlation control for two semiconductor microcavities connected by an optical fiber, *Phys. Scr.* **92**(6) (2017) 065101.
13. A.-B. A. Mohamed, H. Eleuch and C. H. R. Ooi, Non-locality correlation in two driven qubits inside an open coherent cavity: Trace norm distance and maximum bell function, *Sci. Rep.* **9**(1) (2019) 1–10.
14. K. Berrada, A. Chafik, H. Eleuch and Y. Hassouni, Concurrence in the framework of coherent states, *Quantum Inf. Process.* **9**(1) (2010) 13–26.
15. M. Kargarian, R. Jafari and A. Langari, *Phys. Rev. A* **76** (2007) 060304.
16. R. De Wolf, The potential impact of quantum computers on society, *Ethics Inf. Technol.* **19**(4) (2017) 271–276.
17. K. Kan and M. Une, Recent trends on research and development of quantum computers and standardization of post-quantum cryptography, *Monet. Econ. Stud.* **39** (2021) 77–108.
18. B. M. Terhal, Quantum supremacy, here we come, *Nat. Phys.* **14**(6) (2018) 530–531.
19. M. H. Yung, Quantum supremacy: Some fundamental concepts, *Natl. Sci. Rev.* **6**(1) (2019) 22–23.
20. O. H. M. Ross, A review of quantum-inspired metaheuristics: Going from classical computers to real quantum computers, *IEEE Access* **8** (2019) 814–838.
21. E. Farhi and A. W. Harrow, Quantum supremacy through the quantum approximate optimization algorithm, preprint (2016), arXiv:1602.07674.
22. D. Spehner, Quantum correlations and distinguishability of quantum states, *J. Math. Phys.* **55**(7) (2014) 075211.
23. D. Keefer and R. de Vivie-Riedle, Pathways to new applications for quantum control, *Acc. Chem. Res.* **51**(9) (2018) 2279–2286.
24. M. Y. Niu, S. Boixo, V. N. Smelyanskiy and H. Neven, Universal quantum control through deep reinforcement learning, *NPJ Quantum Inf.* **5**(1) (2019) 1–8.
25. D. Bimberg and U. W. Pohl, Quantum dots: Promises and accomplishments, *Mater. Today* **14**(9) (2011) 388–397.
26. T. Zhong, J. Kindem, E. Miyazono and A. Faraon, Nanophotonic quantum memory based on rare-earth-ions coupled to an optical resonator, in *CLEO*: *QELS Fundamental Science* (Optical Society of America, 2015), p. FW3A-3.
27. A. H. Abdel-Aty, H. Kadry, A. B. Mohamed and H. Eleuch, Correlation dynamics of nitrogen vacancy centers located in crystal cavities, *Sci. Rep.* **10**(1) (2020) 1–11.
28. K. Dohnalová, T. Gregorkiewicz and K. Kůsová, Silicon quantum dots: Surface matters, *J. Phys. Condens. Matter* **26**(17) (2014) 173201.
29. E. A. Sete and H. Eleuch, High-efficiency quantum state transfer and quantum memory using a mechanical oscillator, *Phys. Rev. A* **91**(3) (2015) 032309.
30. S. Dhomkar, J. Henshaw, H. Jayakumar and C. A. Meriles, Long-term data storage in diamond, *Science Adv.* **2**(10) (2016) e1600911.
31. C. Lee, W. Yang and R. G. Parr, Development of the Colle-Salvetti correlation-energy formula into a functional of the electron density, *Phys. Rev. B* **37**(2) (1988) 785.
32. F. Jelezko, C. Tietz, A. Gruber, I. Popa, A. Nizovtsev, S. Kilin and J. Wrachtrup, Spectroscopy of

single N-V centers in diamond, *Single Mol.* **2**(4) (2001) 255–260.

33. B. R. Smith, D. W. Inglis, B. Sandnes, J. R. Rabeau, A. V. Zvyagin, D. Gruber and T. Plakhotnik, Five-nanometer diamond with luminescent nitrogen-vacancy defect centers, *Small* **5**(14) (2009) 1649–1653.
34. F. Jelezko, I. Popa, A. Gruber, C. Tietz, J. Wrachtrup, A. Nizovtsev and S. Kilin, Single spin states in a defect center resolved by optical spectroscopy, *Appl. Phys. Lett.* **81**(12) (2002) 2160–2162.
35. R. Schirhagl, K. Chang, M. Loretz and C. L. Degen, Nitrogen-vacancy centers in diamond: Nanoscale sensors for physics and biology, *Annu. Rev. Phys. Chem.* **65** (2014) 83–105.
36. T. Gaebel, I. Popa, A. Gruber, M. Domhan, F. Jelezko and J. Wrachtrup, Stable single-photon source in the near infrared, *New J. Phys.* **6**(1) (2004) 98.
37. Y. Chu and M. D. Lukin, Quantum optics with nitrogen-vacancy centers in diamond, in *Quantum Optics and Nanophtonics*, eds. C. Fabre, V. Sandoghdar, N. Treps and L. F. Cugliandolo (Oxford University Press, UK, 2017), pp. 229–270.
38. T. Wang and Y. Zhang, Scalable multi-qubit quantum gates in quantum networks based on the microtoroidal-resonator-mediated nitrogen-vacancy centers in diamond, *JOSA B* **37**(5) (2020) 1372–1378.
39. P. Siyushev, M. Nesladek, E. Bourgeois, M. Gulka, J. Hruby, T. Yamamoto and F. Jelezko, Photoelectrical imaging and coherent spin-state readout of single nitrogen-vacancy centers in diamond, *Science* **363**(6428) (2019) 728–731.
40. M. Steiner, P. Neumann, J. Beck, F. Jelezko and J. Wrachtrup, Universal enhancement of the optical readout fidelity of single electron spins at nitrogen-vacancy centers in diamond, *Phys. Rev. B* **81**(3) (2010) 035205.
41. G. Waldherr, J. Beck, M. Steiner, P. Neumann, A. Gali, T. Frauenheim and J. Wrachtrup, Dark states of single nitrogen-vacancy centers in diamond unraveled by single shot NMR, *Phys. Rev. Lett.* **106**(15) (2011) 157601.
42. M. V. Hauf, P. Simon, N. Aslam, M. Pfender, P. Neumann, S. Pezzagna, J. A. Garrido, Addressing single nitrogen-vacancy centers in diamond with transparent in-plane gate structures, *Nano Lett.* **14**(5) (2014) 2359–2364.
43. W. L. Yang, Z. Q. Yin, Z. Y. Xu, M. Feng and C. H. Oh, Quantum dynamics and quantum state transfer between separated nitrogen-vacancy centers embedded in photonic crystal cavities, *Phys. Rev. A* **84**(4) (2011) 043849.
44. B. S. Song, S. Noda, T. Asano and Y. Akahane, Ultra-high-Q photonic double-heterostructure nanocavity, *Nat. Mater.* **4**(3) (2005) 207–210.
45. C. Meiar, K. Hennessy, E. D. Haberer, R. Sharma, Y. S. Choi, K. McGroddy and E. L. Hu, Visible resonant modes in GaN-based photonic crystal membrane cavities, *Appl. Phys. Lett.* **88**(3) (2006) 031111.
46. K. Hennessy, A. Badolato, M. Winger, D. Gerace, M. Atatüre, S. Gulde and A. Imamoğlu, Quantum nature of a strongly coupled single quantum dot–cavity system, *Nature* **445**(7130) (2007) 896–899.
47. L. Childress, M. G. Dutt, J. M. Taylor, A. S. Zibrov, F. Jelezko, J. Wrachtrup and M. D. Lukin, Coherent dynamics of coupled electron and nuclear spin qubits in diamond, *Science* **314**(5797) (2006) 281–285.
48. M. Stoneham, Is a room-temperature, solid-state quantum computer mere fantasy? *Physics* **2** (2009) 34.
49. L. Caspani, C. Reimer, M. Kues, P. Roztocki, M. Clerici, B. Wetzel and R. Morandotti, Multifrequency sources of quantum correlated photon pairs on-chip: A path toward integrated Quantum Frequency Combs, *Nanophotonics* **5**(2) (2016) 351–362.
50. X. Xu, J. Wu, M. Tan, T. G. Nguyen, S. T. Chu, B. E. Little and D. J. Moss, Broadband microwave frequency conversion based on an integrated optical micro-comb source, *J. Lightwave Technol.* **38**(2) (2020) 332–338.
51. S. Fasel, F. Robin, E. Moreno, D. Erni, N. Gisin and H. Zbinden, Energy-time entanglement preservation in plasmon-assisted light transmission, *Phys. Rev. Lett.* **94**(11) (2005) 110501.
52. V. S. Erturk, E. Godwe, D. Baleanu, P. Kumar, J. Asad and A. Jajarmi, Novel fractional-order Lagrangian to describe motion of beam on nanowire, *Acta Phys. Polon. A* **140**(3) (2021) 265–272.
53. A. Jajarmi, D. Baleanu, K. Z. Vahid, H. M. Pirouz and J. H. Asad, A new and general fractional Lagrangian approach: A capacitor microphone case study, *Results Phys.* **31** (2021) 104950.
54. A. Jajarmi, D. Baleanu, K. Zarghami Vahid and S. Mobayen, A general fractional formulation and tracking control for immunogenic tumor dynamics, *Math. Methods Appl. Sci.* **45**(2) (2022) 667–680.
55. D. Baleanu, S. Zibaei, M. Namjoo and A. Jajarmi, A nonstandard finite difference scheme for the modeling and nonidentical synchronization of a novel fractional chaotic system, *Adv. Differ. Equ.* **2021**(1) (2021) 1–19.
56. D. Baleanu, M. H. Abadi, A. Jajarmi, K. Z. Vahid and J. J. Nieto, A new comparative study on the general fractional model of COVID-19 with isolation and quarantine effects, *Alex. Eng. J.* **61**(6) (2022) 4779–4791.

57. P. Roztocki, M. Kues, C. Reimer, B. Wetzel, S. Sciara, Y. Zhang and R. Morandotti, Practical system for the generation of pulsed quantum frequency combs, *Opt. Express* **25**(16) (2017) 18940–18949.
58. X. Xu, M. Tan, B. Corcoran, J. Wu, T. G. Nguyen, A. Boes and D. J. Moss, Photonic perceptron based on a Kerr microcomb for high-speed, scalable, optical neural networks, *Laser Photon. Rev.* **14**(10) (2020) 2000070.
59. M. W. Doherty, N. B. Manson, P. Delaney, F. Jelezko, J. Wrachtrup and L. C. L. Hollenber, *Phys. Rep.* **1** (2013) 528.
60. E. P. Wigner and M. M. Yanase, Information Contents of Distributions, *Proc. Natl. Acad. Sci. USA* **49** (1963) 910.
61. S.-X. Wu, J. Zhang, C.-S. Yu and H.-S. Song, Uncertainty-induced quantum nonlocality, *Phys. Lett. A* **378** (2014) 344.
62. G. Vidal and R. F. Werner, A computable measure of entanglement, *Phys. Rev. A* **65** (2002) 032314.
63. W. L. Yang, J. H. An, C. Zhang, M. Feng and C. H. Oh, Preservation of quantum correlation between separated nitrogen-vacancy centers embedded in photonic-crystal cavities, *Phys. Rev. A* **87**(2) (2013) 022312.
64. N. Zidan, H. Bakry and A. U. Rahman, Entanglement and entropic uncertainty of two Two-level atoms, *Ann. Phys.* **534** (2022) 2100555.
65. Y. N. Guo, M. F. Fang, G. Y. Wang and K. Zeng, Generation and protection of steady-state quantum correlations due to quantum channels with memory, *Quantum Inf. Process.* **15**(12) (2016) 5129–5144.
66. A.-B. A. Mohamed, A. U. Rahman and H. Eleuch, Temporal quantum memory and non-locality of two trapped ions under the effect of the intrinsic decoherence: Entropic uncertainty, trace norm nonlocality and entanglement, *Symmetry* **14(**4) (2022) 648.